Ordered Nanoclusters in Lipid-Cholesterol Membranes

Maria K. Ratajczak

Department of Physics, Institute for Biophysical Dynamics, and The James Franck Institute, The University of Chicago, 929 E. 57th Street, Chicago, Illinois 60637, USA

Eva Y. Chi,[†] Shelli L. Frey,[‡] Kathleen D. Cao, Laura M. Luther, and Ka Yee C. Lee[*]

Department of Chemistry, Institute for Biophysical Dynamics, and The James Franck Institute, The University of Chicago, 929 E. 57th Street, Chicago, Illinois 60637, USA

Jaroslaw Majewski

Manuel Lujan Jr. Neutron Scattering Center, Los Alamos Neutron Science Center, Los Alamos National Laboratory, Los Alamos, New Mexico 87545, USA

Kristian Kjaer

Max-Planck Institute of Colloids and Interfaces, Am Mühlenberg, Germany
Niels Bohr Institute, University of Copenhagen, Copenhagen, Denmark

(Received 21 April 2008; published 8 July 2009)

X-ray diffraction of sphingomyelin-dihydrocholesterol (SM-DChol) monolayers revealed short-ranged (~25 Å) 2D ordering. These nanoclusters show two distinct regions: below the cusp point of the phase diagram (35 mol% DChol), a constant d spacing was observed; above the cusp, the d spacing increases linearly with DChol in accordance to Vegard's law for binary alloys. The components in this lipidic alloy are thus a 65:35 SM-DChol entity and excess DChol. Reflectivity data further support the emergence above the cusp of an uncomplexed DChol population with greater vertical mobility.

DOI: 10.1103/PhysRevLett.103.028103 PACS numbers: 87.16.dt

There is increasing evidence that lipids comprising the plasma membrane are inhomogeneously distributed, forming liquid domains rich in cholesterol and saturated lipids. These domains, often referred to as ''lipid rafts'' [1], have been implicated in many cell functions including endocytosis, signaling, and lipid regulation [1,2]. Driving forces for raft formation and the role cholesterol plays on membrane lipid organization remain unresolved. Characterization of lipid heterogeneities have been carried out using giant unilamellar vesicles [3,4] and giant plasma membrane vesicles [5] where large-scale (i.e., multi-μm-scale) fluid-fluid phase separation has been observed. Membrane inhomogeneities, however, have not been unequivocally demonstrated in living cells, perhaps due to their small size and/or dynamic nature [6,7]. Here, we use lipid monolayers composed of different compositions of sphingomyelin (SM, derived from egg, Avanti Polar Lipids) and cholesterol, both of which are thought to be major constituents of lipid rafts, to examine lipid-cholesterol interactions. Grazing-incidence x-ray diffraction (GIXD) and x-ray reflectivity (XR) techniques were used to probe lateral ordering and structural features of these mixed monolayers. The simplicity and wide accessibility of molecular compositions and densities of a lipid monolayer at the air-water interface render it an attractive model system to resolve cholesterol's role in lipid organization [8,9].

Cholesterol modulates the fluidity of lipid membranes by modifying the ordering of lipid acyl chains [10]. In monolayers, cholesterol has been found to specifically interact with high melting-temperature lipids, i.e., sphingolipids, to promote phase separation [8,11,12]. Curiously, the phase diagram of monolayers composed of mixtures of certain lipids and cholesterol or dihydrocholesterol (DChol, Sigma-Aldrich) exhibits two fluid-fluid immiscibility regions [11] and DChol is routinely used instead of cholesterol to avoid oxidative damage [13]. Figure 1 shows the phase diagram of a binary SM-DChol monolayer; the shape of such a phase diagram can be explained by a thermodynamic model of condensed complexes, with the stoichiometry defined by the cusp point location [10,11]. At DChol content below the cusp point, all DChol molecules are associated with SM, forming SM-DChol complexes in the presence of excess SM and giving rise to a fluid-fluid coexistence. Conversely, at DChol content above the cusp point, SM-DChol complexes are in coexistence with excess DChol [11,12]. While there has been limited direct evidence for complex formation, it has been evoked to explain various observations in model lipid membranes [13,14], as well as certain aspects of cholesterol homeostasis in cells [15]. Following our preliminary report of GIXD performed on mixed SM-DChol and dipalmitoylphosphatidylcholine-DChol monolayers [9], we present structural data here that further tests the existence and composition of the proposed complexes.

GIXD experiments, which measure lateral organization, were carried out in a Langmuir trough liquid diffractometer [16] with a pure water subphase at $30 \pm 0.5\,^{\circ}\mathrm{C}$. SM-DChol compositions spanned both immiscibility re-

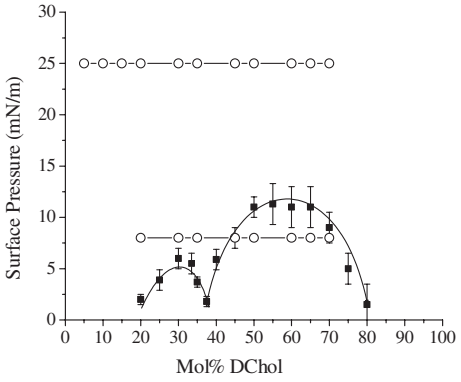

FIG. 1. Fluid-fluid immiscibility phase diagram of binary SM-DChol monolayers on a pure water subphase at 30 °C. The open circles represent compositions and surface pressures used in the current study.

gions of the phase diagram and GIXD data were collected at 8 and 25 mN/m for each lipid composition (Fig. 1). The 8 mN/m pressure corresponds to the region where phase separation on the μm scale is observed by fluorescence microscopy (FM), whereas 25 mN/m is close to bilayer equivalent pressure [17] where a single homogeneous phase is observed [9].

The background subtracted GIXD data for SM-DChol mixtures, ranging from 20 to 100 mol% DChol, at both pressures show a single *Bragg peak* (Fig. 2) with characteristics distinct from either pure DChol or SM. At low DChol content (5–15%), a discernible *Bragg peak* can only be obtained at the higher pressure. Pure DChol exhibits a single *Bragg peak* at both pressures with a d spacing of 5.72 Å, a hexagonal lattice constant, $a_h = 2 \cdot d/(\sqrt{3}) = 6.61$ Å, and an in-plane coherence length, $L_{xy} \sim 75$ Å (Fig. 2). For SM, GIXD shows no *Bragg peak* below

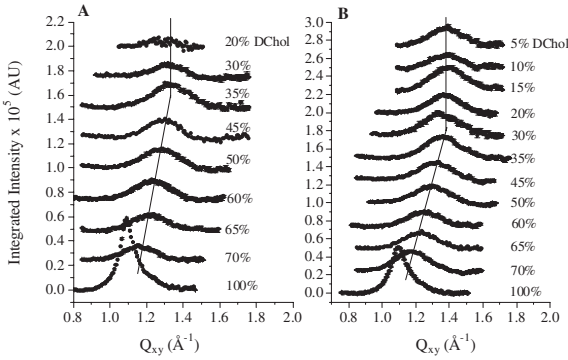

FIG. 2. Background subtracted GIXD peaks for SM-DChol mixtures as a function of DChol content at (a) 8 and (b) 25 mN/m. Q_{xy} is the horizontal scattering vector [29]. The peaks were integrated over the relevant region of the vertical scattering vector Q_z and the data were offset for clarity. The broad peaks indicate a short range ordering that extends ~25 Å. The peak position remains relatively unchanged (vertical lines to guide the eye) for DChol content below 35 mol%, but shifts monotonically (slanted lines) towards smaller Q_{xy} (larger d spacing) with increasing DChol.

30 mN/m, but reveals two peaks at 35 mN/m [9], signifying the packing of tilted SM acyl tails in a distorted hexagonal unit cell. The d spacings associated with the two peaks are $d_{(1,-1)} = 4.29$ and $d_{(0,1)+(1,0)} = 4.61$ Å [$(1, -1)$ and $(1, 0) + (0, 1)$ are the Miller indices], and their L_{xy} values are ~170 and 40 Å, respectively.

While pure SM does not exhibit ordering below 30 mN/m, binary SM-DChol mixtures at both 8 and 25 mN/m show a single Bragg peak with a d spacing close to that of the $(1, 0) + (0, 1)$ peak of pure SM at 35 mN/m; the $(1, -1)$ peak of pure SM, corresponding to a lower d spacing, disappears in all mixtures. Furthermore, the d spacings are different from that of pure DChol, and the corresponding L_{xy} values (~25 Å) are smaller than those of either pure component. The entity giving rise to the scattering in the mixed film is clearly not either pure component.

At a fixed DChol content, GIXD data for the binary mixture at both pressures give rise to diffraction peaks with similar d spacing, integrated intensity, and L_{xy} values. Although μm-scale phase separation is not observed by FM at 25 mN/m, similarities in scattering features observed above and below the mixing-demixing line demonstrate that nanoscale ordered structures present at low surface pressures persist to higher pressures. Moreover, all of the diffraction peaks have coherence lengths ranging from 21 to 25 Å, pointing to their nanoscopic and perhaps dynamic nature.

Figure 3 shows d spacing values as a function of DChol content. Not surprisingly, d spacing values obtained at 25 mN/m are slightly lower than those obtained at 8 mN/m (Fig. 3). The d spacing-DChol composition plot (Fig. 3) clearly shows two different regimes. At DChol content below 35 mol%, the d spacing corresponding to that of the pure SM $(1, 0) + (0, 1)$ peak remains roughly the same, albeit with a lower L_{xy} value, irrespective of the amount of DChol (Fig. 3). However, at DChol content higher than 35 mol%, the d spacing value increases linearly with increasing DChol for both pressures.

The change in d spacing with compositions has been reported in other binary systems, such as metal alloys. In such a system, the crystal lattice constant [18] changes from that of component 1 to that of component 2 linearly, as described by the empirical Vegard's law [19]. For SM-DChol mixtures, such a linear relationship only holds for DChol content greater than 35 mol%. Casting our data in light of Vegard's law, component 1 of the lipidic alloy is not pure SM, but rather the scattering entity present at 35 mol% DChol, with component 2 being the excess DChol. Interpreting these results in the context of the complex formation model, the cusp point at 35 mol% DChol marks the stoichiometric ratio of the complexes, where all SM molecules are associated with DChol.

Vegard's law was first found to adequately describe the relationship between lattice parameters and composition in metal alloys, where the elements are noninteracting and

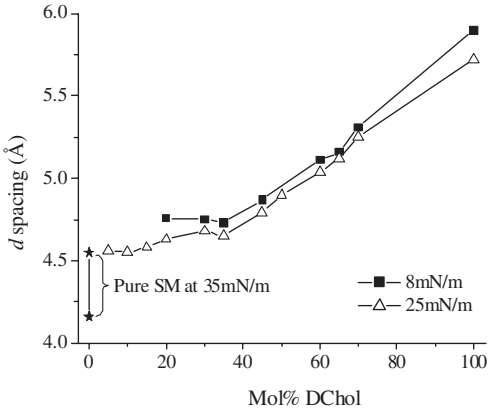

FIG. 3. *d* spacing versus composition plot of DChol in SM-DChol mixtures at 8 and 25 mN/m. The *d* spacing varies linearly with DChol content above 35 mol% DChol. Pure SM at 35 mN/m (filled stars) exhibits distorted hexagonal packing resulting in two diffraction peaks and therefore two *d* spacing values; no peak is observed for pure SM at 8 and 25 mN/m.

thus ideally mixing [19]. It has been applied to successfully predict lattice parameters of binary alloys based on known lattice constants of the constituent elements [20]. This predictive power of Vegard's law has been demonstrated in other systems, including lipid mixtures. Dorset and Pangborn [21] showed that the characteristic packing dimensions of a cholesteryl ester solid solution, cholesteryl undecanoate–cholesteryl laurate, can be predicted by Vegard's law from the values of the pure components. Unlike the SM-DChol system presented here, Vegard's law holds for the entire composition range in their case, indicating ideal mixing. It is clear that the peculiar behavior observed in the SM-DChol system, where two distinct regimes exist in the *d* spacing-composition plot, does not occur in all binary lipid systems. When the two components in the binary alloy are interacting, nonideal mixing ensues. The lack of a linear dependence of *d* spacing with composition at low DChol content therefore suggests interactions between SM and DChol. The fact that ordering of SM at 25 mN/m emerges only when DChol is present points to attractive interactions between the two. This condensing effect of DChol is consistent with the notion that cholesterol tends to rigidify fluid lipid films [10].

Lipid bilayers composed of cholesterol and two other lipids show a closed-loop liquid immiscibility. Similarly, a three component alloy, such as Bi-Sb-Cu, also exhibits a closed-loop liquid immiscibility region [12,22], where the phase behavior of this alloy can be understood in terms of complex formation between Cu and Sb [22]. The parallel between the metallic and the lipidic systems thus argues for the existence of similar lipid-cholesterol complexes in lipid mixtures. As shown in Fig. 3, the linear relationship holds only in the 35–100 mol% DChol range, pointing to a SM-DChol scattering entity with the cusp point revealing its stoichiometry. The constant *d* spacing at low DChol concentrations up to the cusp point arises from the ordered lipid-cholesterol entity with excess unordered lipid not affecting the *Bragg peak* position. At higher DChol concentration, the system can be likened to that of a Vegard metal alloy with the SM-DChol complex and DChol acting as primary and secondary components and the linear increase in *d* spacing due to lattice mismatch between the two.

GIXD data suggest that DChol can exist in a complexed or an uncomplexed state depending on the DChol content. Earlier work examining the uptake of DChol by β-cyclodextrin (β-CD) has shown that at DChol content below the cusp point, desorption of DChol by β-CD is low whereas the opposite is true above the cusp point [13,14,23]. The β-CD data are in agreement with the 2-state model of DChol, with the cusp as the demarcation point [13]. The high DChol uptake at high DChol content could be due to greater vertical translational freedom of uncomplexed cholesterol, capable of penetrating into the lipid headgroup region and availing themselves to β-CD.

To locate the vertical position of DChol within the SM-DChol film, XR measurements were made to obtain out-of-plane electron density (ED) distributions [24]. Pure DChol can be modeled using 2 slabs (1: sterol ring; 2: aliphatic chain), each with a unique ED, thickness, and interfacial roughness. Similarly, pure SM can be modeled using two slabs (1: headgroups, 2: acyl tails). For SM-DChol mixtures, satisfactory fit is obtained only when ED distribution is extended to three slabs (1: partial SM headgroup–DChol sterol ring, 2: partial SM headgroup–partial SM tailgroup–DChol sterol ring, and 3: SM tail–DChol acyl chain) (see supplementary material [25]). ED values of the SM headgroup region, slab 1, as a function of DChol content are

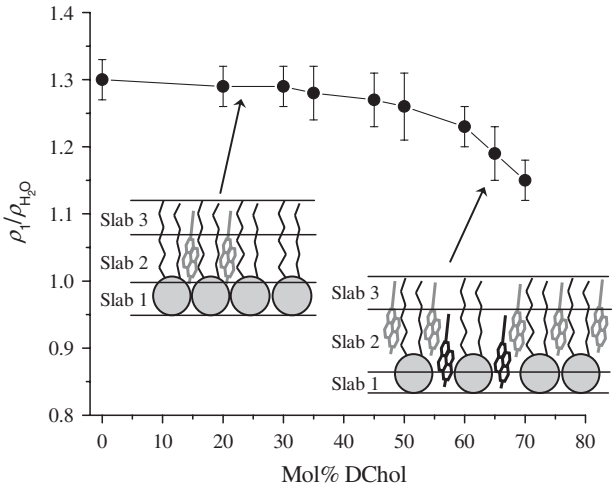

FIG. 4. Dependence of normalized ED of slab 1, normalized to the ED of water, $\rho_{H_2O} = 0.334\ e^-/Å^3$, ρ_1/ρ_{H_2O}, (defined as the SM headgroup region) on DChol content. Values of ρ_1 were obtained from fitting the XR data. The cartoons illustrate that ρ_1 decreases with the penetration of DChol into the headgroup region at high DChol content, since ED of the DChol sterol ring is lower than that of the lipid headgroup. Gray DChol denote complexed DChol and black DChol denote free DChol with higher vertical mobility.

shown in Fig. 4. As shown, ED of slab 1 decreases with increasing DChol due to the mixing of the lower ED DChol sterol rings into the higher ED SM headgroups. This decrease, however, is not linear: it is modest at low DChol content, but the rate of decrease is larger for higher DChol content. At low DChol content, DChol is localized in the SM tailgroup region, exerting little effect on the SM headgroup ED. With the relatively large cross sectional area of SM headgroup compared to its tailgroup, DChol can be readily accommodated in the predominantly SM film without perturbing the headgroup region (illustration in Fig. 4). In contrast, a more pronounced decrease in the ED of slab 1 is found with increasing DChol beyond the cusp point (Fig. 4), consistent with DChol penetrating into SM headgroups, which lowers the ED of the region (illustration in Fig. 4). These results are also consistent with the proposed enhanced out-of-plane translational motion of uncomplexed DChol molecules [26].

The GIXD and XR data presented here demonstrate that when mixed with SM, DChol exists in two different states, with the cusp point separating the two. At low DChol content, favorable interactions between SM and DChol yield a unique ordered structure that is short-ranged [27,28]. Below the cusp point, the d spacing remains roughly constant and DChol is primarily localized in the SM tailgroup region, irrespective of DChol content. Above the cusp point, a linear increase in d spacing with increasing DChol follows Vegard's law. The fact that Vegard's law holds only at DChol content above the cusp point indicates that the two constituents in this ''lipidic alloy'' system are not the pure components, but rather a SM-DChol complex and excess DChol. The greater out-of-plane mobility of DChol revealed by XR further adds credence to the existence of an uncomplexed DChol population beyond the cusp point. The short-ranged order suggests a dynamic nature of these nanoclusters, and is in line with some recent critical fluctuation interpretations of lipid rafts [6]. The underlying molecular interactions that drive the formation of SM-DChol nanoclusters should be generally applicable to other lipid-cholesterol systems.

This work was supported by the NSF (No. MCB-0616249). We acknowledge beamtime on BW1 in HASYLAB, DESY and support from the International Institute for Complex Adaptive Matter (NSF Grant No. DMR 0645461) for the x-ray experiments. M. K. R. is grateful for the support from the Burroughs Wellcome Fund (No. 1001774), E. Y. C. from the NIH (No. AG025649) and the March of Dimes (No. 6-FY07-357), and S. L. F. from the NSF. J. M. was supported by Los Alamos National Laboratory under DOE Contract No. W7405-ENG-36 and the DOE Office of Basic Energy Science.

*Address reprint requests and inquiries to Ka Yee C. Lee: kayeelee@uchicago.edu

†Current address: Department of Chemical and Nuclear Engineering and the Center for Biomedical Engineering, University of New Mexico, 222 University Blvd. NE, Albuquerque, NM 87131

‡Current address: Department of Chemistry, Gettysburg College, 300 N. Washington Street, Gettysburg, PA 17325

[1] K. Simons and E. Ikonen, Nature (London) **387**, 569 (1997).
[2] M. Edidin, Annu. Rev. Biophys. Biomol. Struct. **32**, 257 (2003).
[3] J. Korlach *et al.*, Proc. Natl. Acad. Sci. U.S.A. **96**, 8461 (1999).
[4] S. L. Veatch and S. L. Keller, Phys. Rev. Lett. **89**, 268101 (2002).
[5] T. Baumgart *et al.*, Proc. Natl. Acad. Sci. U.S.A. **104**, 3165 (2007).
[6] S. L. Veatch *et al.*, Proc. Natl. Acad. Sci. U.S.A. **104**, 17650 (2007).
[7] W. K. Subczynski *et al.*, Biophys. J. **92**, 1573 (2007).
[8] A. Radhakrishnan, T. G. Anderson, and H. M. McConnell, Proc. Natl. Acad. Sci. U.S.A. **97**, 12422 (2000).
[9] C. Ege *et al.*, Biophys. J. **91**, L01 (2006).
[10] T. P. McMullen, R. N. Lewis, and R. N. McElhaney, Curr. Opin. Colloid Interf. Sci. **8**, 459 (2004).
[11] A. Radhakrishnan and H. M. McConnell, Biophys. J. **77**, 1507 (1999).
[12] A. Radhakrishnan and H. McConnell, Proc. Natl. Acad. Sci. U.S.A. **102**, 12662 (2005).
[13] A. Radhakrishnan and H. M. McConnell, Biochemistry **39**, 8119 (2000).
[14] M. K. Ratajczak *et al.*, Biophys. J. **93**, 2038 (2007).
[15] Y. Lange, J. Ye, and T. L. Steck, Proc. Natl. Acad. Sci. U.S.A. **101**, 11664 (2004).
[16] J. Majewski *et al.*, Chem. Eur. J. **1**, 304 (1995).
[17] A. Seelig, Biochim. Biophys. Acta **899**, 196 (1987).
[18] Because of the linear relationship between the principal (1, 0), (0, 1), and (1, −1) d spacings for the hexagonal unit cell and the resulting lattice constant, a_h, we discuss the Vegard's law in terms of d spacings instead of lattice constants.
[19] L. Vegard, Z. Phys. **5**, 17 (1921).
[20] W. B. Pearson, *Handbook of Lattice Spacings and Structures of Metals* (Pergamon Press, Oxford, 1967).
[21] D. L. Dorset and W. A. Pangborn, Proc. Natl. Acad. Sci. U.S.A. **89**, 1822 (1992).
[22] H. Janecke, *Handbuch aller Legierungen* (R. Kiepert, Berlin, 1940).
[23] A. Radhakrishnan *et al.*, Biochim. Biophys. Acta **1511**, 1 (2001).
[24] J. Als-Nielsen and K. Kjaer, NATO Advanced Study Institutes B 211, 113 (1989).
[25] See EPAPS Document No. E-PRLTAO-103-003928 for supplementary material. For more information on EPAPS, see http://www.aip.org/pubservs/epaps.html.
[26] Y. Lange, J. Ye, and T. L. Steck, J. Biol. Chem. **280**, 36126 (2005).
[27] M. D. Collins and S. L. Keller, Proc. Natl. Acad. Sci. U.S.A. **105**, 124 (2008).
[28] T. Baumgart, S. T. Hess, and W. W. Webb, Nature (London) **425**, 821 (2003).
[29] T. R. Jensen and K. Kjaer, *Novel Methods to Study Interfacial Layers* (Elsevier, Amsterdam, 2001), p. 205.